CrossMark

electronic reprint

Journal of
Applied Crystallography
ISSN 1600-5767

On identification of symmetric and improperly quasi-symmetric grain boundaries

Krzysztof Glowinski

J. Appl. Cryst. (2014). **47**, 726–731

Copyright © International Union of Crystallography

Author(s) of this paper may load this reprint on their own web site or institutional repository provided that this cover page is retained. Republication of this article or its storage in electronic databases other than as specified above is not permitted without prior permission in writing from the IUCr.

For further information see http://journals.iucr.org/services/authorrights.html

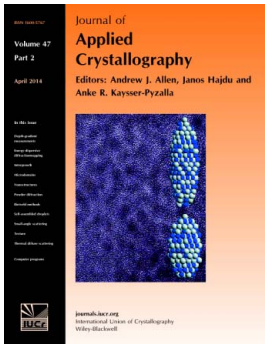

Many research topics in condensed matter research, materials science and the life sciences make use of crystallographic methods to study crystalline and non-crystalline matter with neutrons, X-rays and electrons. Articles published in the *Journal of Applied Crystallography* focus on these methods and their use in identifying structural and diffusion-controlled phase transformations, structure-property relationships, structural changes of defects, interfaces and surfaces, *etc.* Developments of instrumentation and crystallographic apparatus, theory and interpretation, numerical analysis and other related subjects are also covered. The journal is the primary place where crystallographic computer program information is published.

Crystallography Journals Online is available from **journals.iucr.org**

Journal of
Applied Crystallography
ISSN 1600-5767

Received 13 October 2013
Accepted 25 February 2014

On identification of symmetric and improperly quasi-symmetric grain boundaries

Krzysztof Glowinski

Institute of Metallurgy and Materials Science, Polish Academy of Sciences, Reymonta 25, 30-059, Kraków, Poland. Correspondence e-mail: kglowinski@ymail.com

Symmetric and improperly quasi-symmetric grain boundaries have special geometric features. They are important reference boundaries in quantitative studies of boundary networks. Methods for identification of symmetric and improperly quasi-symmetric boundaries used so far, which are based on distance functions defined in the space of boundary parameters, are computationally complex and inefficient. In this article, new parameters that approximate the distances to the nearest symmetric and improperly quasi-symmetric boundaries are defined to simplify and speed up the analyses. Very strong correlations between the new parameters and the corresponding distances validate these new parameters to be a suitable replacement for the distances. Distributions of the introduced parameters may serve as characteristics of boundary networks. As an example, the new parameters are applied to the studies of symmetric and improperly quasi-symmetric characters of boundaries in three-dimensional microstructure data collected from a nickel-based superalloy.

© 2014 International Union of Crystallography

1. Introduction

Although it is a known fact that many properties of polycrystalline materials are affected by grain boundaries, this influence still remains to be completely understood. Boundaries need to be characterized in three dimensions and from both atomic scale and 'macroscopic' (geometric) viewpoints. While at the atomic level only limited studies are feasible, the three-dimensional boundary geometry (*i.e.* misorientations between neighboring crystallites and indices of boundary planes) can be determined for a significant number of boundaries. Since three-dimensional experimental techniques utilizing automated serial sectioning (Groeber *et al.*, 2006; Uchic *et al.*, 2012) and X-ray tomography (Hefferan *et al.*, 2009; Poulsen, 2012) have advanced considerably in recent years, it is possible to collect boundary data sets large enough for carrying out some statistical studies of boundary networks (Saylor *et al.*, 2003; Groeber *et al.*, 2008; Rohrer *et al.*, 2010).

One expects the impact of distinct boundaries on the properties of polycrystals to be different. On the basis of the geometric parameters, several groups of boundaries of special geometry are distinguishable; there are, for example, twist, tilt, symmetric and improperly quasi-symmetric (IQS) boundaries.[1] Geometrically special boundaries are frequently used as reference boundaries in various analyses concerning grain boundaries (Amouyal *et al.*, 2005; Rowenhorst & Voorhees, 2005; Beladi & Rohrer, 2013; Glowinski & Morawiec, 2013). Therefore, efficient methods for recognizing the boundaries of such characteristic geometries in large data sets are needed. Different approaches to the description of twist and tilt boundaries have been thoroughly discussed by Morawiec & Glowinski (2013). In this article, the previous studies are extended with methods for identification of symmetric and IQS boundary characters.

Assuming the presence of an inversion center, symmetric and IQS boundaries are equivalent to 180° twists and 180° tilts, respectively (Morawiec, 2012). In practice, registered boundary parameters are affected by experimental errors which must be taken into account. So far, symmetric and IQS boundaries have been recognized on the basis of distance functions defined in the space of macroscopic boundary parameters. Briefly, with a properly defined metric (Cahn & Taylor, 2006; Olmsted, 2009; Morawiec, 2009), two boundaries of similar geometric attributes are close and those significantly different are distant. If the distance δ_S (δ_I) from the investigated boundary to the nearest symmetric (IQS) boundary is smaller than an assumed limit (determined by the experimental resolution), then the boundary is qualified as near-symmetric (near-IQS), *cf.* Glowinski & Morawiec (2012) and Glowinski (2013). Computation of the accurate distances is, however, complex. As a consequence, the time needed for the processing of large boundary data sets becomes very long.

In this article, it is proposed to replace the distances by their easy to calculate approximations. First, the new parameters α_S and α_I are defined as a measure of closeness of the geometry of a given boundary to symmetric and IQS configurations, respectively. In the next step, the correlations between α_S and δ_S and between α_I and δ_I are examined. From the high level of

[1] There are also the classifications into small- and large-angle boundaries, and into coincidence-site lattice (CSL) boundaries, but they do not take into account boundary plane parameters.

electronic reprint

these correlations, it becomes evident that the introduced parameters are a reliable substitute for the distances.

Probability density functions (PDFs) and cumulative distribution functions (CDFs) for α_S and α_I may serve as characteristics of a given boundary network, which supplement five-parameter grain boundary distributions like those presented by Saylor *et al.* (2003) and Rohrer *et al.* (2010). Deviations in PDFs computed for experimental boundary data from the reference PDFs obtained for randomly generated boundaries (*i.e.* for the isotropic case) will reveal if some boundary geometries, either close to or distant from symmetric and IQS configurations, are preferred or disfavored in a given microstructure. From the corresponding CDFs, the fractions of near-symmetric and near-IQS boundaries can be read for arbitrary limiting distances (resolutions), *cf.* Glowinski (2013). Below, the reference distribution functions for α_S and α_I are presented for the cubic $m\bar{3}m$, hexagonal $6/mmm$, tetragonal $4/mmm$ and orthorhombic mmm holohedral symmetries. Then, to give a practical example of how the reference data can be used in analysis of experimentally registered boundary networks, the random PDFs are compared with those computed for three-dimensional data of boundaries in nickel-based superalloy IN100.

2. Parameters α_S and α_I

With the correspondence between symmetric and 180°-twist boundaries and between IQS and 180°-tilt boundaries, the task of identifying near-symmetric and near-IQS boundaries simplifies to the verification of whether there exists a symmetrically equivalent representation of a given boundary with an explicit near-twist or near-tilt character, respectively, and with the misorientation angle ω close to 180° at the same time.

Computation of properly defined distances[2] to the nearest twist (δ_N) and nearest tilt (δ_L) boundaries is complex – it requires running numerical optimization algorithms. However, in a recent article (Morawiec & Glowinski, 2013), the parameters $\alpha_N = \min(90^\circ - \alpha)$ and $\alpha_L = \min(\alpha)$ were introduced as an alternative measure of closeness of a given boundary to a pure twist and to a pure tilt, respectively ($\alpha = \arccos|\mathbf{u}\cdot\mathbf{n}|$, $\mathbf{u}$ denotes the misorientation axis, $\mathbf{n}$ is the boundary plane normal and the minimization is over the values obtained for all representations of that boundary). It was shown that these parameters are strongly correlated with the corresponding distances, so they can substitute for δ_N and δ_L. Moreover, their calculation times are significantly shorter than those for the distances and the codes are much simpler.

The question now arises on how to modify the parameters α_N and α_L to obtain new parameters that could replace the distances δ_S and δ_I to the nearest symmetric and IQS boundaries, respectively. Let us define $\alpha_S = \min\{[\alpha^2 + (180^\circ - \omega)^2]^{1/2}\}$ and $\alpha_I = \min\{[(90^\circ - \alpha)^2 + (180^\circ - \omega)^2]^{1/2}\}$; as in the case of α_N and α_L, the minimization is over all boundary representations. These parameters combine the terms allowing for recognizing near-twist and near-tilt characters of boundary representations, respectively, and the terms describing how large are the differences of the misorientation angles from 180°. Similarly to α_N and α_L, α_S and α_I are affected by neither inversion nor grain exchange symmetries.

To confirm that α_S and α_I can replace the distances δ_S and δ_I providing similar results, pairs $\{\delta_S, \alpha_S\}$ and $\{\delta_I, \alpha_I\}$ have been computed for 10^6 random grain boundaries for the cubic symmetry case. The correlations between α_S and δ_S and between α_I and δ_I are very strong; they are illustrated in Fig. 1. Based on numerical experiments, the maximum relative difference between α_S and δ_S (α_I and δ_I) is 0.4% (33.3%), while the average deviation is 0.08% (5.7%). It is observed that α_I parameters are generally slightly lower than those of δ_I. The corresponding PDFs and CDFs for α_S and α_I are compared with the analogous functions for δ_S and δ_I in Fig. 2. The distributions for α_S are practically identical to those for δ_S. In the case of α_I and δ_I, the widths of the PDFs are similar, whereas the mean value of α_I (12.9°) is slightly shifted toward lower values compared to the mean of δ_I (13.6°). According to

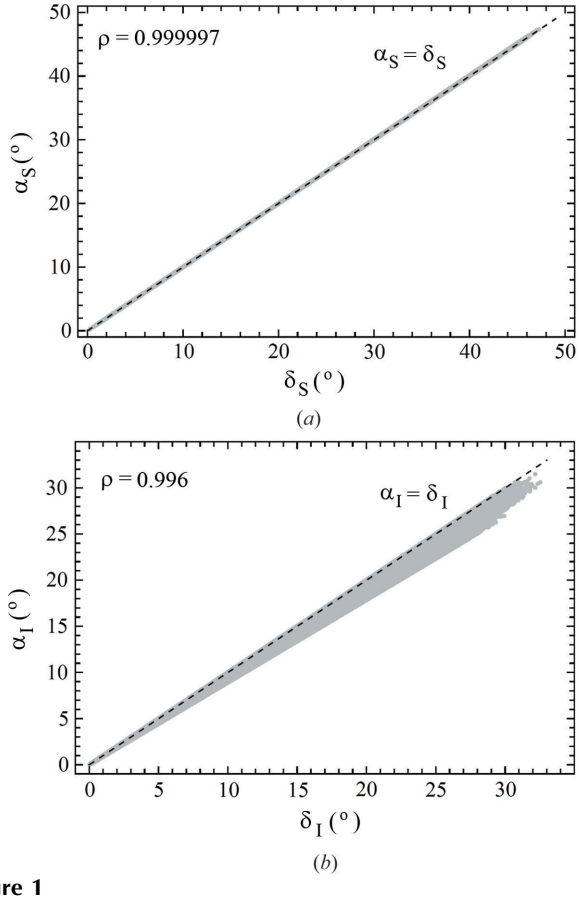

Figure 1
(*a*) Parameters α_S and distances δ_S to the nearest symmetric boundaries. (*b*) Parameters α_I and distances δ_I to the nearest improperly quasi-symmetric boundaries. Displayed data correspond to the cubic symmetry case and were computed for 10^6 random boundaries. Symbols ρ denote the corresponding Spearman rank correlation coefficients.

[2] In this article, we consider the same metric as in the earlier works (Glowinski & Morawiec, 2013, 2012; Morawiec & Glowinski, 2013; Glowinski, 2013): the distance between two boundaries is given as $[\chi^2 + (\xi_1^2 + \xi_2^2)/2]^{1/2}$, where χ describes the difference in their misorientations, and ξ_i ($i = 1, 2$) are the angles between the adequate boundary normals.

electronic reprint

the above results, the distances to the nearest symmetric and IQS boundaries can be approximated by α_S and α_I, respectively, and a given boundary will be classified as symmetric (IQS) if α_S (α_I) is below an assumed limit.

3. Symmetric and IQS boundaries in a nickel-based alloy

The above random distribution functions will be used as a point of reference in analysis of experimentally collected boundary data. Our results complete those of Morawiec & Glowinski (2013) with the analysis of symmetric and IQS characters of boundaries in the data set `Small IN100` provided by M. A. Groeber. These data were acquired from the Ni-based superalloy IN100 using the three-dimensional electron backscatter diffraction technique. A full description of the material, stages of its processing and details of the experimental setup are given by Groeber *et al.* (2006). Alignment of successive slices, data clean-up and reconstruction of boundary surfaces in the form of triangular meshes were carried out using the *DREAM.3D* (http://dream3d.bluequartz.net) program. The surface reconstruction (and smoothing) algorithms leave non-smooth triple lines (see Fig. 3). Although the mesh segments directly neighboring these lines constitute about 40% of all segments, they were excluded from further analysis because it was noticed that they lead to significant artifacts in the distribution of boundary planes. The resulting mesh consists of about 1.2×10^4 distinct grain boundaries made up from about 1.5×10^6 triangular segments.

In the studied material, a significant fraction of all boundaries are Σ3 coherent twin boundaries with (111) boundary planes. The twin boundaries are simultaneously symmetric and IQS; hence, in the experimental distributions, elevated values (compared to those for random boundaries) are expected for α_S and α_I close to zero. In Fig. 4(*a*), the PDF (weighted by mesh segment areas) for α_S obtained for the boundaries in the superalloy is compared with that for random boundaries. Because of the shapes of the curves, it is difficult to read from the graphs whether boundaries of small α_S are over- or underrepresented in the alloy, so the information is incomplete. Therefore, the experimental distribution of α_S is also expressed as multiples of the random distribution (MRD) (see Fig. 4*b*). Analogous distributions for α_I are shown in Figs. 4(*c*) and 4(*d*). Indeed, the plots indicate that near-symmetric and near-IQS boundaries are overrepresented: the values at $\alpha_S \simeq 0$ and $\alpha_I \simeq 0$ are 48 and 10.5 MRD, respectively. Since twin boundaries dominate in this microstructure, analogous distributions are computed for the subset of the data consisting only of boundaries whose misorientations deviate by more than 5° from the Σ3 misorientation (Figs. 4*b* and 4*d*). With such a threshold, all near-twin boundaries (28.4% of all boundaries) are effectively removed. This allows for determination of the contribution of near-symmetric and near-IQS boundaries other than those close to the twin boundary. The anisotropy observed in the data with Σ3 boundaries excluded is weaker than that in the complete data: the values at $\alpha_S \simeq 0$ and $\alpha_I \simeq 0$ are 1.5 and 1.6 MRD, respectively.

In the distributions of grain boundaries obtained for the investigated alloy (Rohrer *et al.*, 2010), apart from a very

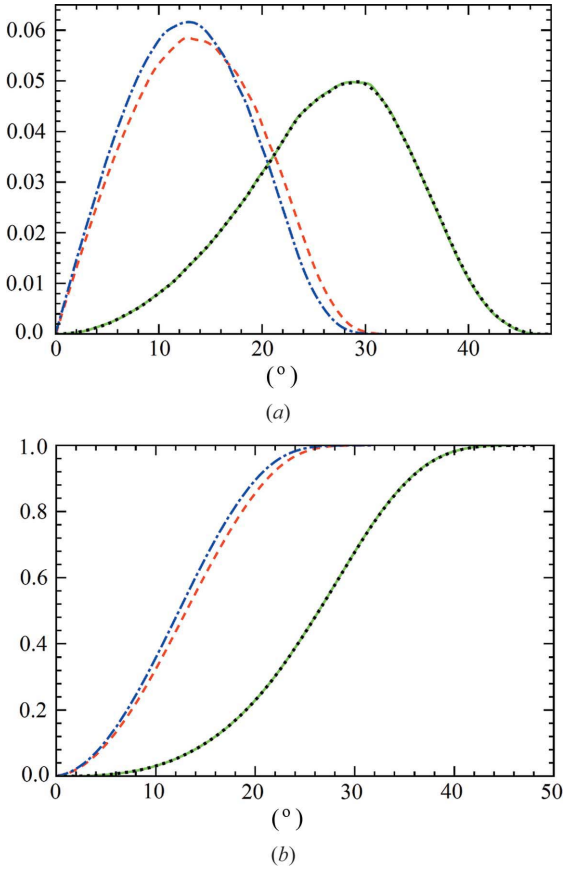

Figure 2
Probability density functions (*a*) and the corresponding cumulative distribution functions (*b*) for the distances δ_S (green solid line) and δ_I (red dashed line) to the nearest symmetric and improperly quasi-symmetric boundaries, respectively, and for the new parameters α_S (black dotted line) and α_I (blue dash–dotted line). The functions correspond to the cubic symmetry case and were obtained based on 10^6 random boundaries.

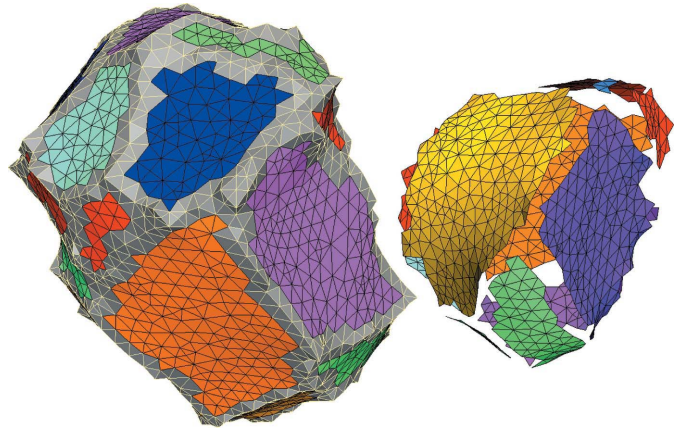

Figure 3
Visualization (http://www.paraview.org) of boundaries of selected grains reconstructed in the form of triangular meshes; different colors are related to distinct boundaries. In the left-hand side grain, the segments neighboring the triple lines (excluded from the analysis) are shaded gray.

electronic reprint

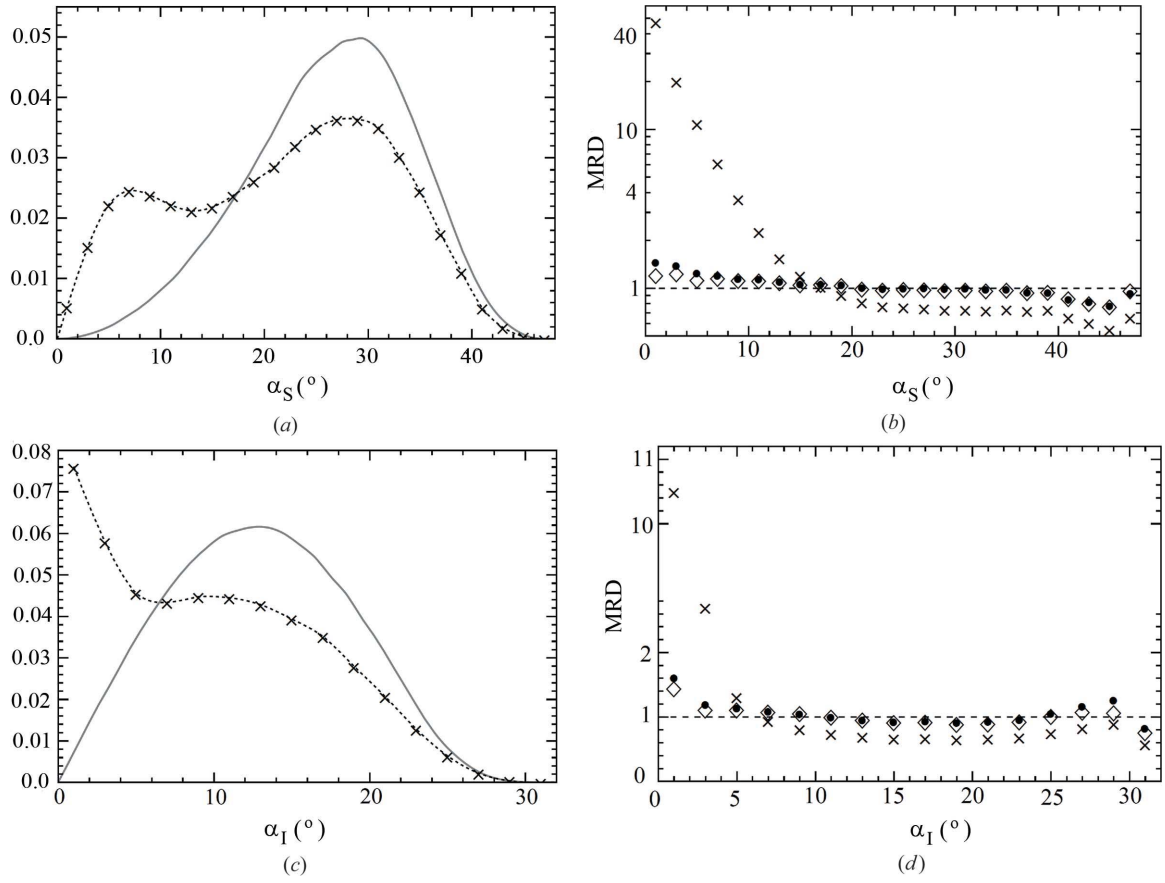

Figure 4
Probability density functions for the parameters α_S (*a*) and α_I (*c*); in (*a*) and (*c*), solid lines correspond to random boundaries, and crosses to experimental data of the Ni-based alloy. Distributions of α_S (*b*) and α_I (*d*) for the superalloy expressed as multiples of random distributions; in (*b*) and (*d*), crosses correspond to the complete data set, discs to the data with Σ3 boundaries excluded, and diamonds to the subset without low-Σ and Σ27*a* CSL boundaries. For computation of the experimental distributions, 2° bins were used.

strong maximum at Σ3/(111) related to coherent twins, smaller peaks were observed at the Σ7/(111) and Σ9/(1$\bar{1}$4) boundaries, which are both IQS, and the latter is also symmetric. This makes it sensible to ask about the percentage of high-coincidence boundaries among all symmetric and IQS boundaries, so the distributions of α_S and α_I are also computed for a subset which does not contain (assuming the threshold of 5°) low-Σ ($3 \leq \Sigma \leq 11$) and Σ27*a*[3] CSL boundaries (32.1% of all boundaries). Clearly, the deviations of these distributions from the random data are decreased compared to the first subset: the values at $\alpha_S \simeq 0$ and $\alpha_I \simeq 0$ are 1.2 and 1.4 MRD, respectively (Figs. 4*b* and 4*d*). It can be seen that near-symmetric and near-IQS boundaries other than those with the low-Σ and Σ27*a* CSL misorientations are overrepresented in the boundary network.

The fractions of symmetric and IQS boundaries can be read from the corresponding CDFs. Assuming a limit for α_S and α_I of say 8°,[4] the fractions of symmetric and IQS boundaries among random grain boundaries are 1.4 and 21.9%, respectively (Fig. 2*b*). In the Ni-based alloy, they are respectively, 13.5 and 44.6% for the complete data set, 1.7 and 25.2% for the subset without Σ3 boundaries, and 1.6 and 24.8% for the data with low-Σ and Σ27*a* CSL boundaries removed.

Besides the maxima at $\alpha_S \simeq 0 \simeq \alpha_I$, the distributions are relatively flat with values below one MRD for $\alpha_S > 15°$ and $\alpha_I > 7°$, respectively. These broad minima result from the normalization of probability: data above one MRD must be balanced by data below one MRD; if the peak height is decreased (like in the distributions for the subset without Σ3 boundaries), then the minimum becomes shallow. In the distributions for superalloy IN100, no maxima occur for large α_S and α_I values, but this is not a general rule. For instance, in a recent analysis (Glowinski & Morawiec, 2013) of the distributions of WC/WC boundaries in the WC–Co composites (Kim *et al.*, 2008), it turned out that the two most frequent boundary types are far from the nearest symmetric boundaries, namely with α_S at 30 and 79.4°; since the fractions of boundaries of these types are significant, peaks in the corresponding distribution will appear.

It is worth noting that with the parallel implementation (Glowinski & Morawiec, 2012), calculation of α_S and α_I for all 1.5×10^6 segments took about three minutes on an eight-core personal computer, whereas the calculation time for the

[3] Σ27*a* boundaries are excluded as they tend to occur at triple junctions where Σ3 boundaries intersect Σ9 boundaries.
[4] Since the resolution for grain misorientations is about 1°, this choice for the used metric is based mainly on the resolution for boundary plane parameters; *e.g.* Saylor *et al.* (2003) estimated it to be no better than 7.5°.

electronic reprint

distances δ_S and δ_I is about 52 h. At this point, another way of speeding up of data processing should be mentioned: reconstructed meshes can be simplified by merging coplanar segments (Dillard *et al.*, 2007). However, for the purpose of identification of symmetric and IQS boundaries, it is much easier to take advantage of the new parameters α_S and α_I.

4. Non-cubic symmetries

The correlations between the parameters α_S and α_I and the corresponding distances δ_S and δ_I, respectively, have also been analyzed for hexagonal, tetragonal and orthorhombic holohedries. These correlations are at the same level as those in the cubic case. Thus, α_S and α_I are also applicable to investigations of boundary networks in materials of these non-cubic symmetries. The corresponding reference PDFs for α_S and α_I are presented in Fig. 5; 10^6 random boundaries for each of the three symmetries were generated to obtain these curves. As was pointed out by Glowinski (2013), the lower the symmetry (the smaller the number of equivalent boundary representations, and the lower the chances to satisfy the conditions for a boundary to be geometrically special), the smaller the fractions of boundaries with special geometry (assuming the same limiting distance).

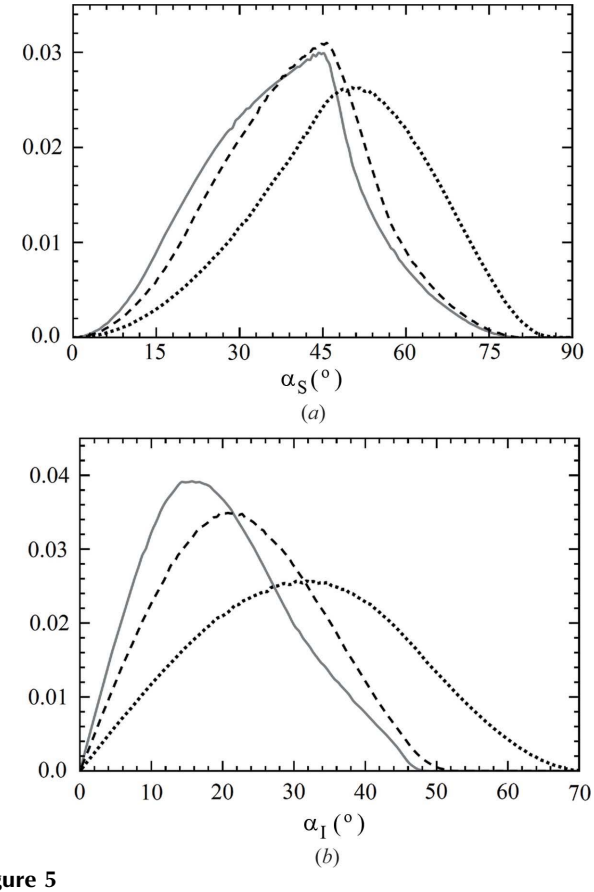

Figure 5
Probability density functions for the parameters α_S (*a*) and α_I (*b*) for hexagonal, tetragonal and orthorhombic holohedral symmetries plotted using gray solid, black dashed and black dotted lines, respectively.

5. Summary

In this report, the alternative parameters α_S and α_I have been introduced to approximate the distances δ_S and δ_I to the nearest symmetric and IQS boundaries, respectively. The correlations between the newly defined parameters and the distances have been examined, and since they are at a very high level, the new parameters are a reliable replacement for δ_S and δ_I. Furthermore, α_S and α_I can be calculated in times significantly shorter than those for the distances. This allows for a reduction of the time needed for identification of symmetric and IQS boundaries in large boundary data sets.

Distributions of α_S and α_I may be used as tools for microstructure characterization. The distribution functions for α_S and α_I obtained for random boundaries in the cases of several holohedral symmetries have been presented. These functions will be used as a reference basis for further studies of experimental data sets. To give an example, the random data have been compared with analogous distributions obtained for three-dimensional electron backscatter diffraction data of Ni-based superalloy IN100. In this material, boundaries of both α_S and α_I close to zero are expected to be overrepresented because of the high population of $\Sigma3/(111)$ twin boundaries and the elevated number of $\Sigma7/(111)$ and $\Sigma9/(1\bar{1}4)$ boundaries; these three types of boundaries belong to either or both of the considered groups. Therefore, two subsets of these data have also been processed: the first with $\Sigma3$ boundaries excluded and the second one without CSL boundaries of Σ values equal to 3, 5, 7, 9, 11 and 27*a*. In particular, from the distributions corresponding to the second subset, it can be read that the fractions of symmetric and IQS boundaries different from high-coincidence boundaries are increased compared to the random data. Similar analyses of symmetric and IQS characters of boundaries can be carried out for other materials of various holohedral symmetries.

The author is grateful to M. A. Groeber (US Air Force Research Laboratory) for permission to use the `Small IN100` data set. This work was supported by the European Union under the European Social Fund within project No. POKL.04.01.00-00-004/10.

References

Amouyal, Y., Rabkin, E. & Mishin, Y. (2005). *Acta Mater.* **53**, 3795–3805.
Beladi, H. & Rohrer, G. S. (2013). *Metall. Mater. Trans. A*, **44**, 115–124.
Cahn, J. W. & Taylor, J. E. (2006). *J. Mater. Sci.* **41**, 7669–7674.
Dillard, S. E., Bingert, J., Thoma, D. & Hamann, B. (2007). *IEEE Trans. Vis. Comput. Graph.* **13**, 1528–1535.
Glowinski, K. (2013). *Solid State Phenom.* **203–204**, 427–430.
Glowinski, K. & Morawiec, A. (2012). *Proceedings of the 1st International Conference on 3D Materials Science*, edited by M. De Graef, H. F. Poulsen, A. Lewis, J. Simmons & G. Spanos, pp. 119–124. Wiley.
Glowinski, K. & Morawiec, A. (2013). *J. Mater. Sci.* doi:10.1007/s10853-013-7958-5.
Groeber, M., Ghosh, S., Uchic, M. D. & Dimiduk, D. M. (2008). *Acta Mater.* **56**, 1257–1273.

electronic reprint

Groeber, M. A., Haley, B. K., Uchic, M. D., Dimiduk, D. M. & Ghosh, S. (2006). *Mater. Charact.* **57**, 259–273.
Hefferan, C. M., Li, S. F., Lind, J., Lienert, U., Rollett, A. D., Wynblatt, P. & Suter, R. M. (2009). *Comput. Mater. Continua*, **14**, 209–219.
Kim, C.-S., Massa, T. R. & Rohrer, G. S. (2008). *J. Am. Ceram. Soc.* **91**, 996–1001.
Morawiec, A. (2009). *J. Appl. Cryst.* **42**, 783–792.
Morawiec, A. (2012). *Z. Kristallogr.* **227**, 199–206.
Morawiec, A. & Glowinski, K. (2013). *Acta Mater.* **61**, 5756–5767.
Olmsted, D. L. (2009). *Acta Mater.* **57**, 2793–2799.
Poulsen, H. F. (2012). *J. Appl. Cryst.* **45**, 1084–1097.
Rohrer, G. S., Li, J., Lee, S., Rollett, A. D., Groeber, M. & Uchic, M. D. (2010). *Mater. Sci. Technol.* **26** 661–669.
Rowenhorst, D. J. & Voorhees, P. W. (2005). *Metall. Mater. Trans. A*, **36**, 2127–2135.
Saylor, D. M., Morawiec, A. & Rohrer, G. S. (2003). *Acta Mater.* **51**, 3663–3674.
Uchic, M., Groeber, M., Shah, M., Callahan, P., Shiveley, A., Scott, M., Chapman, M. & Spowart, J. (2012). *Proceedings of the 1st International Conference on 3D Materials Science*, edited by M. De Graef, H. F. Poulsen, A. Lewis, J. Simmons & G. Spanos, pp. 195–202. Wiley.

electronic reprint